Publication Year	2018
Acceptance in OA@INAF	2020-09-29T10:46:54Z
Title	An Efficient 2.5-D Finite-Element Approach Based on Transformation Optics for the Analysis of Elliptical Horns
Authors	Gentili, Gian Guido; Khosronejad, Misagh; NESTI, Renzo; Pelosi, Giuseppe; Selleri, Stefano
DOI	10.1109/TAP.2018.2851289
Handle	http://hdl.handle.net/20.500.12386/27521
Journal	IEEE TRANSACTIONS ON ANTENNAS AND PROPAGATION
Number	66

An Efficient 2.5D Finite Element Approach Based on Transformation Optics for the Analysis of Elliptical Horns

G.G. Gentili, M. Khosronejad, R. Nesti, G. Pelosi, S. Selleri

***Abstract*—This paper describes a new method to analyze elliptical horns. The method is based on a coordinate transformation that maps the elliptical shape to a circular shape, allowing to use 2.5D Body of Revolution (BoR) Finite Element Method (FEM) formulation with a greatly improved efficiency over 3D methods. Applications are shown to the analysis and design of shaped arbitrary axial ratio horns.**

Keywords: ***Finite Element Method, elliptical horns, body-of-revolution.***

I. Introduction

Rectangular and Elliptical horns are interesting solutions when non symmetrical beams are needed, as in the case of primary feed of shaped reflectors for earth coverage or radars [1], [2], [3], [4], [5]. In some cases, when very low cross-polar levels are required, e.g. when circular polarization is used, the smooth-wall horn is replaced by a corrugated horn or a dielectric core horn [2]. Radiation from elliptical apertures have been also exploited for opposite reasons, i.e. to symmetrize the main beam [6].

In spite of the superior performances of elliptical horns with respect to rectangular horns in terms of side-lobes [5], the difficulty in the analysis has always been an obstacle to the full exploitation of such structures, even if closed formulas have been found to represent the field radiated by elliptical apertures [9]. Some papers dealing with modeling of radiation from elliptical horns are available [7], [8], but, for a full-wave analysis of elliptical horns, nowadays one must resort to full 3D techniques, such as 3D FEM [10], or Multiple Multipole expansion [8] in conjunction with the Mode-Matching method. These methods are CPU demanding, since a 3D discretization of the overall structure must be carried out. Mode-matching can be successfully used for the inner problem using Mathieu functions to represent the modal fields [11], [12], and this is probably the most efficient technique in case of corrugated horns, but for smooth-walled horns it becomes quite inefficient, since the smooth wall must be discretized in a large number of elliptical waveguide steps. Moreover, even in the case of corrugated horns, coupling to the exterior problem is an issue, since it requires coupling to some full 3D method to represent the field outside.

G.G. Gentili, M. Khosrnonejad are with Politecnico di Milano, Dipartimento di Elettronica, Informazione e Bioingegneria, p.za L. da Vinci 32, Milano (Italy). mailto: gianguido.gentili@polimi.it. R. Nesti is with INAF, Osservatorio di Arcetri, Largo E. Fermi 5, Firenze (Italy). G. Pelosi and S. Selleri are with Università di Firenze, Dipartimento di Ingegneria dell'Informazione, 50139, Firenze (Italy).

A further disadvantage limiting the use of elliptical horns reported in the literature is its manufacturing [1]. However, owing to technological improvements in classical processes and to the advent of additive manufacturing techniques, the realization of such structures is feasible and cheap [13], [14].

The purpose of this paper is therefore to discuss a very efficient method developed for the analysis of elliptical horns. The method is based on the concept of Transformations Optics (TO) [15]. Thanks to the use of a very simple transformation, the elliptical geometry is converted to a circular one, and this is solved by a 2D FEM by a Body-of-Revolution (BoR) formulation [16], [17]. The use of very few circular harmonics allows an accurate representation of the original fields in the elliptical geometry, leading to an extremely efficient code.

The formulation of the method is discussed in section II-III, whereas in section IV we show some numerical results and design examples. Finally, some conclusions are presented, in which we enlighten some possible developments of the technique.

II. Transformations Optics

The concept of general coordinate transformations in the frame of Maxwell's equations is well known, and it found application in, to cite a few, cloaking [18], antenna pattern manipulation [19] and, in Finite-Differences or Finite-Element analysis, to develop "perfect" absorbing boundaries, the so-called Perfectly Matched Layer (PML) [20].

Let's assume to have a starting, or "original", system of coordinates (x', y', z') and a second, or "transformed" system of coordinates (x, y, z) linked by

$$x = x(x', y', z') \tag{1}$$

$$y = y(x', y', z') \tag{2}$$

$$z = z(x', y', z') \tag{3}$$

with an associated Jacobian matrix

$$\mathbf{J} = \begin{bmatrix} \frac{\partial x}{\partial x'} & \frac{\partial x}{\partial y'} & \frac{\partial x}{\partial z'} \\ \frac{\partial y}{\partial x'} & \frac{\partial y}{\partial y'} & \frac{\partial y}{\partial z'} \\ \frac{\partial z}{\partial x'} & \frac{\partial z}{\partial y'} & \frac{\partial z}{\partial z'} \end{bmatrix}. \tag{4}$$

If $\mathbf{e}'$ and $\mathbf{h}'$ are the solution of Maxwell's equation for a given problem in the original coordinate frame x', y', z', with material parameters characterized by tensors $\boldsymbol{\epsilon}'$ and $\boldsymbol{\mu}'$, then if in the transformed frame (x, y, z) the material properties are set to

$$\boldsymbol{\epsilon}_r = \frac{\mathbf{J}\boldsymbol{\epsilon}_r'\mathbf{J}^{\mathrm{T}}}{\det \mathbf{J}} \tag{5}$$

$$\boldsymbol{\mu}_r = \frac{\mathbf{J}\boldsymbol{\mu}'_r\mathbf{J}^{\mathrm{T}}}{\det \mathbf{J}} \tag{6}$$

the electric and magnetic fields $\mathbf{e}$ and $\mathbf{h}$ in frame (x, y, z) and those in the original frame are related by

$$\mathbf{e}' = \mathbf{J}^{\mathrm{T}}\mathbf{e} \tag{7}$$

$$\mathbf{h}' = \mathbf{J}^{\mathrm{T}}\mathbf{h}. \tag{8}$$

The above transformations pave the way to a set of interesting possible applications, but in our case the purpose is focused to convert the elliptical geometry to a circular one, for which efficient tools for the analysis can be applied. Let's assume an elliptical structure is present in the original frame, extending from coordinate z'_1 to z'_2. The elliptical structure is characterized by z-dependent semiaxes $a = a(z')$ and $b = b(z')$ along x' and y' respectively. The axial ratio is therefore dependent on z'. This allows to include in the analysis structures whose cross-section is variable, for example, from circular to elliptical.

Now we apply the following transformations:

$$\begin{aligned} x &= \frac{x'}{s_x(z')} \\ y &= \frac{y'}{s_y(z')} \\ z &= z' \end{aligned} \tag{9}$$

in which

$$s_x(z) = \begin{cases} \frac{a(z_1)}{b(z_1)} & \text{for} \quad z \le z_1 \\ \frac{a(z)}{b(z_1)} & \text{for} \quad z_1 < z < z_2 \\ \frac{a(z_2)}{b(z_1)} & \text{for} \quad z \ge z_2 \end{cases} \tag{10}$$

$$s_y(z) = \begin{cases} 1 & \text{for} \quad z \le z_1 \\ \frac{b(z)}{b(z_1)} & \text{for} \quad z_1 < z < z_2 \\ \frac{b(z_2)}{b(z_1)} & \text{for} \quad z \ge z_2 \end{cases} \tag{11}$$

where we used the fact that $z' = z$. Transformations (9)–(11) convert ellipses in (x', y') plane to circles in (x, y) plane with radius $b(z_1)$. The Jacobian is

$$\mathbf{J} = \begin{bmatrix} \frac{1}{s_x} & 0 & -\frac{x}{s_x}\frac{ds_x}{dz} \\ 0 & \frac{1}{s_y} & -\frac{y}{s_y}\frac{ds_y}{dz} \\ 0 & 0 & 1 \end{bmatrix}. \tag{12}$$

It is straightforward to compute $\det(\mathbf{J}) = \frac{1}{s_x s_y}$ and we find from (5)-(6) that isotropic material parameters ϵ'_r, μ'_r in the original frame transform, in frame (x, y, z), to the following anisotropic parameters

$$\boldsymbol{\epsilon}_r = \epsilon'_r\boldsymbol{\Lambda} \tag{13}$$

$$\boldsymbol{\mu}_r = \mu'_r\boldsymbol{\Lambda} \tag{14}$$

with

$$\boldsymbol{\Lambda} = \begin{bmatrix} \frac{s_y}{s_x} + \frac{s_y}{s_x}d_x^2x^2 & d_xd_yxy & -s_yd_xx \\ d_xd_yxy & \frac{s_x}{s_y} + \frac{s_x}{s_y}d_y^2y^2 & -s_xd_yy \\ -s_yd_xx & -s_xd_yy & s_xs_y \end{bmatrix} \tag{15}$$

where $d_x = \frac{ds_x}{dz}$, $d_y = \frac{ds_y}{dz}$.

We hence obtain a problem that is 'equivalent' to the original problem, but the structure is now circular and filled with anisotropic materials. Solving the problem in frame (x, y, z) allows to easily derive the fields in the original frame. It is clear that the set of transformation represented by (9)–(11) has a great advantage: a BoR formulation based on a 2D mesh can be used to solve the problem ([16], [17]). As shown in the following sections, this provides a dramatic speed-up with respect to full 3D analysis.

III. BoR-FEM formulation

In order to apply BoR-FEM we switch to a cylindrical coordinate system (ρ, ϕ, z) and express the anisotropy in cylindrical coordinates:

$$\boldsymbol{\Lambda}_{\mathrm{cyl}} = \mathbf{R}\boldsymbol{\Lambda}\mathbf{R}^{\mathrm{T}} \tag{16}$$

where

$$\mathbf{R} = \begin{bmatrix} \cos\phi & \sin\phi & 0 \\ -\sin\phi & \cos\phi & 0 \\ 0 & 0 & 1 \end{bmatrix} \tag{17}$$

is the rotation matrix. Setting $x = \rho\cos\phi$, $y = \rho\sin\phi$ one finds that the terms in matrix $\boldsymbol{\Lambda}_{\mathrm{cyl}}$ can be expressed as a sum of products of functions of (ρ, z) times functions of ϕ. Setting $\cos\phi = c_\phi$, $\sin\phi = s_\phi$ one finds

$$\begin{aligned} \Lambda_{\rho\rho} = \quad & \tfrac{s_y}{s_x}c_\phi^2 + \tfrac{s_y}{s_x}d_x^2\rho^2c_\phi^4 + \tfrac{s_x}{s_y}s_\phi^2 + \tfrac{s_x}{s_y}d_y^2\rho^2s_\phi^4 + \\ & 2d_xd_y\rho^2c_\phi^2s_\phi^2 \end{aligned} \tag{18}$$

$$\begin{aligned} \Lambda_{\rho\phi} = \quad & \left(\tfrac{s_x}{s_y} - \tfrac{s_y}{s_x}\right)c_\phi s_\phi + \rho^2\left(\tfrac{s_x}{s_y}d_y^2 - d_xd_y\right)c_\phi s_\phi^3 + \\ & \rho^2\left(-\tfrac{s_y}{s_x}d_x^2 + d_xd_y\right)c_\phi^3 s_\phi \end{aligned} \tag{19}$$

$$\Lambda_{\rho z} = -d_xs_y\rho c_\phi^2 - d_ys_x\rho s_\phi^2 \tag{20}$$

$$\begin{aligned} \Lambda_{\phi\phi} = \quad & \rho^2\left(\tfrac{s_x}{s_y}d_y^2 + \tfrac{s_y}{s_x}d_x^2 - 2d_xd_y\right)c_\phi^2s_\phi^2 + \\ & \tfrac{s_x}{s_y}c_\phi^2 + \tfrac{s_y}{s_x}s_\phi^2 \end{aligned} \tag{21}$$

$$\Lambda_{\phi z} = \rho\left(d_xs_y - d_ys_x\right)c_\phi s_\phi \tag{22}$$

$$\Lambda_{zz} = s_xs_y \tag{23}$$

and omitted terms are readily found because of the symmetry of $\boldsymbol{\Lambda}$. Note that the generic component ξ, η of tensor $\boldsymbol{\Lambda}_{\mathrm{cyl}}$ can be expressed as

$$\Lambda_{\xi,\eta} = \sum_k \Lambda'_{(k)\xi,\eta}(\rho, z)\Lambda''_{(k)\xi,\eta}(\phi) \tag{24}$$

and similarly, letting $\boldsymbol{\Lambda}^{-1} = \mathbf{V}$

$$V_{\xi,\eta} = \sum_k V'_{(k)\xi,\eta}(\rho, z)V''_{(k)\xi,\eta}(\phi) \tag{25}$$

and this is very useful, since, as is shown in the following section, 3D integrals can be split as a sum of surface integrals (ρ, z) times integrals in ϕ.

We chose the electric-field formulation of FEM (but very similar expressions are obtained for the magnetic field formulation). The weak form suitable for FEM discretization is then [10]

$$\mathcal{A}(\mathbf{t}, \mathbf{e}) - k_0^2\mathcal{B}(\mathbf{t}, \mathbf{e}) = j\omega\mu_0\mathcal{C}(\mathbf{t}, \mathbf{h}_0) \tag{26}$$

where

$$\mathcal{A}(\mathbf{t},\mathbf{e}) = \int_V \nabla\times\mathbf{t}\cdot\boldsymbol{\mu}_r^{-1}\cdot\nabla\times\mathbf{e}\,dV \tag{27}$$

$$\mathcal{B}(\mathbf{t},\mathbf{e}) = \int_V \mathbf{t}\cdot\boldsymbol{\epsilon}_r\cdot\mathbf{e}\,dV \tag{28}$$

$$\mathcal{C}(\mathbf{t},\mathbf{h}) = \int_{\partial V} \mathbf{t}\cdot(\mathbf{i}_\nu\times\mathbf{h}_0)\,dS \tag{29}$$

being $k_0^2 = \omega^2\mu_0\epsilon_0$, $\mathbf{t}$ a generic testing function, $\mathbf{e}$ the unknown electric field, $\mathbf{h}_0$ the applied magnetic field at the boundary and $\mathbf{i}_\nu$ the outward drawn normal unit vector.

We apply Galerkin's method for the discretization of (26). A set of expansion functions is introduced to represent the electric field:

$$\mathbf{e} = \sum_u v_u\mathbf{t}_u \tag{30}$$

and the same set is used for testing. We obtain a system of linear equations that can be expressed as follows:

$$\left(\mathbf{A} - k_0^2\mathbf{B}\right)\mathbf{v} = j\omega\mu_0\mathbf{C}. \tag{31}$$

where we have grouped all expansion coefficients v_u in vector $\mathbf{v}$ and where, from (27)–(29)

$$\mathbf{A}(u,v) = \int_V \nabla\times\mathbf{t}_u\cdot\boldsymbol{\mu}_r^{-1}\cdot\nabla\times\mathbf{t}_v\,dV \tag{32}$$

$$\mathbf{B}(u,v) = \int_V \mathbf{t}_u\cdot\boldsymbol{\epsilon}_r\cdot\mathbf{t}_v\,dV \tag{33}$$

$$\mathbf{C}(u) = \int_{\partial V} \mathbf{t}_u\cdot(\mathbf{i}_\nu\times\mathbf{h}_0)\,dS. \tag{34}$$

Using a normalized modal excitation at the input, we can obtain the generalized impedance matrix $\mathbf{Z}$ description of the scattering problem. It is obtained as:

$$\mathbf{Z} = j\omega\mu_0\mathbf{C}^{\mathrm{T}}\left(\mathbf{A} - \omega^2\mu_0\epsilon_0\mathbf{B}\right)^{-1}\mathbf{C} \tag{35}$$

and the generalized scattering matrix (GSM) as:

$$\mathbf{S} = \mathbf{Z}_w(\mathbf{Z}+\mathbf{Z}_w)^{-1}(\mathbf{Z}-\mathbf{Z}_w)\mathbf{Y}_w \tag{36}$$

where $\mathbf{Z}_w$ is the modal wave impedance and $\mathbf{Y}_w = \mathbf{Z}_w^{-1}$.

A. Computation of matrix elements

In this section we present the details of the computation of matrix elements. In order to take advantage of BoR geometry, we express the electric field as

$$\mathbf{e}^t(\rho,\phi,z) = \sum_{m=1,3,5\cdots}^{M}\sum_q v_q^{t,(m)}\boldsymbol{\tau}_q(\rho,z)c_{m\phi} \tag{37}$$

$$e^\phi(\rho,\phi,z) = \sum_{m=1,3,5\cdots}^{M}\sum_q v_q^{\phi,(m)}\frac{N_q(\rho,z)}{\rho}s_{m\phi} \tag{38}$$

where superscript 't' indicates transverse component (ρ-z plane), superscript 'ϕ' indicates ϕ component, $\boldsymbol{\tau}_q$ are edge elements vector basis functions [10], N_q are Lagrange nodal elements, $c_{m\phi} = \cos m(\phi-\phi_0)$ and $s_{m\phi} = \sin m(\phi-\phi_0)$ represent the azimuthal dependence of the field expansion and where $v_q^{t,(m)}$ and $v_q^{\phi,(m)}$ are unknown expansion coefficients. Setting $\phi_0 = 0$ or $\pi/2$ allows to analyze both possible polarizations at the input. Note that by symmetry considerations, in the series of circular harmonics only odd terms are present. Note also that the series has been truncated to a maximum index M. Because of the excellent behavior for the isotropic case, the functions used are the same as in [17].

We can now introduce a convenient matrix partitioning for matrices $\mathbf{A}$, $\mathbf{B}$ and $\mathbf{C}$ as follows

$$\mathbf{A} = \begin{bmatrix} \mathbf{A}^{(1,1)} & \mathbf{A}^{(1,3)} & \dots & \mathbf{A}^{(1,M)} \\ \mathbf{A}^{(3,1)} & \mathbf{A}^{(3,3)} & \dots & \mathbf{A}^{(3,M)} \\ \dots & \dots & \dots & \dots \\ \mathbf{A}^{(M,1)} & \mathbf{A}^{(M,3)} & \dots & \mathbf{A}^{(M,M)} \end{bmatrix} \tag{39}$$

$$\mathbf{B} = \begin{bmatrix} \mathbf{B}^{(1,1)} & \mathbf{B}^{(1,3)} & \dots & \mathbf{B}^{(1,M)} \\ \mathbf{B}^{(3,1)} & \mathbf{B}^{(3,3)} & \dots & \mathbf{B}^{(3,M)} \\ \dots & \dots & \dots & \dots \\ \mathbf{B}^{(M,1)} & \mathbf{B}^{(M,3)} & \dots & \mathbf{B}^{(M,M)} \end{bmatrix} \tag{40}$$

$$\mathbf{C}^{\mathrm{T}} = \begin{bmatrix} \mathbf{C}^{(1)} & \mathbf{C}^{(3)} & \dots & \mathbf{C}^{(M)} \end{bmatrix} \tag{41}$$

where each term represents a submatrix coupling two circular harmonics. In the known term, each submatrix represents a specific harmonic excitation. For a general TE/TM circular waveguide expansion, the complete expression of the known term is given in the appendix. The generic submatrix with superscript (m,n) can be further partitioned as

$$\mathbf{A}^{(m,n)} = \begin{bmatrix} \mathbf{A}_{tt}^{(m,n)} & \mathbf{A}_{t\phi}^{(m,n)} \\ \mathbf{A}_{\phi t}^{(m,n)} & \mathbf{A}_{\phi\phi}^{(m,n)} \end{bmatrix} \tag{42}$$

$$\mathbf{B}^{(m,n)} = \begin{bmatrix} \mathbf{B}_{tt}^{(m,n)} & \mathbf{B}_{t\phi}^{(m,n)} \\ \mathbf{B}_{\phi t}^{(m,n)} & \mathbf{B}_{\phi\phi}^{(m,n)} \end{bmatrix} \tag{43}$$

$$\mathbf{C}^{(m)} = \begin{bmatrix} \mathbf{C}_t^{(m)} \\ \mathbf{C}_\phi^{(m)} \end{bmatrix} \tag{44}$$

where the subscripts 't' or 'ϕ' refer to testing (first subscript) and expansion functions (second subscript) respectively 't'-directed (ρ-z plane) or 'ϕ'-directed.

From the specific testing/expansion function expressions we obtain

$$\begin{aligned} \nabla\times\boldsymbol{\tau}_q c_{m\phi} &= -\mathbf{i}_\rho\frac{m}{\rho}\tau_{z,q}s_{m\phi} + \\ &+\mathbf{i}_\phi(\partial_z\tau_{\rho,q} - \partial_\rho\tau_{z,q})c_{m\phi} + \mathbf{i}_z\frac{m}{\rho}\tau_{\rho,q}s_{m\phi} = \\ &= \mathbf{i}_\rho D_{\rho,q}^{t,(m)}s_{m\phi} + \mathbf{i}_\phi D_{\phi,q}^{t,(m)}c_{m\phi} + \mathbf{i}_z D_{z,q}^{t,(m)}s_{m\phi} \end{aligned} \tag{45}$$

$$\begin{aligned} \nabla\times\mathbf{i}_\phi\frac{N_q}{\rho}s_{m\phi} &= -\mathbf{i}_\rho\frac{\partial_z N_q}{\rho}s_{m\phi} + \mathbf{i}_z\frac{\partial_\rho N_q}{\rho}s_{m\phi} = \\ &= \mathbf{i}_\rho D_{\rho,q}^{\phi}s_{m\phi} + \mathbf{i}_z D_{z,q}^{\phi}s_{m\phi} \end{aligned} \tag{46}$$

where we introduced functions $D_{\xi,q}^{t,(m)}$ and $D_{\xi,q}^{\phi}$, representing the ρ-z dependence of the generic ξ component of the curl of $\boldsymbol{\tau}_q c_{m\phi}$ and $\mathbf{i}_\phi(N_q/\rho)s_{m\phi}$ respectively. Letting then $\mu_r' = 1$ we have $\boldsymbol{\mu}_r^{-1} = \boldsymbol{\Lambda}^{-1} = \mathbf{V}$ and we can now define the generic coefficient p,q in the characteristic matrices. For an easier notation we use indexed coordinates $\xi_1 = \rho$, $\xi_2 = \phi$, $\xi_3 = z$. Finally, we let $g_{i,m}^t$ and $g_{i,m}^\phi$ represent $c_{m\phi}$ or $s_{m\phi}$ according

to the curl component in (45), (46). As an example, coefficient p, q of matrix $\mathbf{A}_{tt}^{(m,n)}$ is then

$$\mathbf{A}_{tt}^{(m,n)}(p,q) = \sum_i \sum_j \sum_k \int_S D_{\xi_i,p}^{t,(m)} V'_{(k)\xi_i\xi_j} D_{\xi_j,q}^{t,(n)} \rho d\rho dz \cdot \int_0^{2\pi} g_{i,m}^t V''_{(k)\xi_i\xi_j} g_{j,n}^t d\phi \tag{47}$$

therefore

$$\mathbf{A}_{tt}^{(m,n)}(p,q) = \sum_i \sum_j \sum_k \Omega_{ijk}^{A_{tt}}(p,q) \Phi_{ijk}^{A_{tt}}(m,n) \tag{48}$$

in which $\Omega_{ijk}^{A_{tt}}$ represent integrals in (ρ, z) plane and $\Phi_{ijk}^{A_{tt}}$ are integrals in ϕ. Surface integrals do not depend on m and n (a part of multiplying constants) and they are used repeatedly to build the entire matrices of FEM. The complete expressions for the various matrix elements are shown in Appendix A. From the previous expression, a further advantage of the present approach is quite apparent: 3D integrals are reduced to 2D integrals over a 2D mesh since integrals in ϕ can be obtained analytically. Although this is not strictly necessary in the computer implementation, it represents a dramatic speed-up in the assembly of the final matrix system.

B. PML

Since we are mostly interested in radiating structures, absorbing PML conditions have been derived for the case of cylindrical coordinates in an anisotropic medium. We followed the approach outlined in [21], although in our case the material is anisotropic and represented by symmetric tensors $\boldsymbol{\epsilon}_r$ and $\boldsymbol{\mu}_r$. In stretched cylindrical coordinates, the components of the curl are

$$(\nabla \times \mathbf{e})_\rho = \frac{1}{\tilde{\rho}} \frac{\partial e_z^c}{\partial \phi} - \frac{\partial e_\phi^c}{\partial \tilde{z}} \tag{49}$$

$$(\nabla \times \mathbf{e})_\phi = \frac{\partial e_\rho^c}{\partial \tilde{z}} - \frac{\partial e_z^c}{\partial \tilde{\rho}} \tag{50}$$

$$(\nabla \times \mathbf{e})_z = \frac{1}{\tilde{\rho}} \left[\frac{\partial (\tilde{\rho} e_\phi^c)}{\partial \tilde{\rho}} - \frac{\partial e_\rho^c}{\partial \phi} \right] \tag{51}$$

where we defined the stretched coordinates as

$$\tilde{\rho} = \rho_0 + \int_{\rho_0}^{\rho} S_\rho \rho' d\rho' \tag{52}$$

$$\tilde{z} = z_0 + \int_{z_0}^{z} S_z z' dz' \tag{53}$$

so that

$$\frac{\partial}{\partial \tilde{\rho}} = \frac{1}{S_\rho} \frac{\partial}{\partial \rho}, \quad \frac{\partial}{\partial \tilde{z}} = \frac{1}{S_z} \frac{\partial}{\partial z}. \tag{54}$$

Now since

$$-j\omega\mu_0 \boldsymbol{\mu}_{r,\mathrm{cyl}} \cdot \mathbf{h}^c = \nabla \times \mathbf{e}^c \tag{55}$$

if we define $S_\phi = \tilde{\rho}/\rho$ and

$$\mathbf{P} = \begin{bmatrix} S_z S_\phi & 0 & 0 \\ 0 & S_z S_\rho & 0 \\ 0 & 0 & S_\phi S_\rho \end{bmatrix}, \tag{56}$$

$$\boldsymbol{\Sigma} = \begin{bmatrix} S_\rho & 0 & 0 \\ 0 & S_\phi & 0 \\ 0 & 0 & S_z \end{bmatrix} \tag{57}$$

virtually perfect absorbing PML are obtained with a material

$$\boldsymbol{\epsilon}_{r,\mathrm{cyl}}^{\mathrm{PML}} = \mathbf{P} \boldsymbol{\epsilon}_{r,\mathrm{cyl}} \boldsymbol{\Sigma}^{-1} = \mathbf{P} \boldsymbol{\Lambda} \boldsymbol{\Sigma}^{-1} \tag{58}$$

$$\boldsymbol{\mu}_{r,\mathrm{cyl}}^{\mathrm{PML}} = \mathbf{P} \boldsymbol{\Lambda} \boldsymbol{\Sigma}^{-1}. \tag{59}$$

Eq. (58), (59) can be used in any anisotropic material in which we wish to use a BoR-FEM formulation, as in our case. The stretching parameters S_ρ, S_ϕ and S_z have been defined as in [16] and, as usual, accuracy is limited only by numerical discretization. In all our simulated results we found an excellent behavior of the previously defined PML.

C. Radiation

Radiation fields for the structure can be obtained by the equivalence theorem [22]. Letting $\mathbf{e}$, $\mathbf{h}$ be the fields obtained by solving the BoR-FEM problem, the fields in the original structure $\mathbf{e}'$, $\mathbf{h}'$ are obtained as

$$\mathbf{e}' = \mathbf{J}^{\mathrm{T}} \mathbf{e} \tag{60}$$

$$\mathbf{h}' = \mathbf{J}^{\mathrm{T}} \mathbf{h} \tag{61}$$

and points in the transformed domain x, y, z correspond to $x' = s_x x$, $y' = s_y y$, $z' = z$. The equivalent surface currents in the original frame are therefore

$$\mathbf{j}_s' = \mathbf{n}' \times \mathbf{h}' \tag{62}$$

$$\mathbf{m}_s' = -\mathbf{n}' \times \mathbf{e}' \tag{63}$$

where

$$\mathbf{n}' = \frac{\mathbf{J}^{\mathrm{T}} \mathbf{n}}{|\mathbf{J}^{\mathrm{T}} \mathbf{n}|}. \tag{64}$$

Standard radiation integrals can be used to compute the far field and the antenna parameters. Because of the BoR-FEM formulation, the fields can be computed simply along a line in the transformed domain and the equivalent sources computation is therefore very fast. We have

$$\mathbf{e} = \sum_m \sum_q v_q^{t,(m)} \boldsymbol{\tau}_q c_{m\phi} + \mathbf{i}_\phi \sum_m \sum_q v_q^{\phi,(m)} \frac{N_q}{\rho} s_{m\phi} \tag{65}$$

$$\mathbf{h} = -\frac{1}{j\omega\mu_0} \boldsymbol{\mu}_r^{-1} \sum_m \sum_q v_q^{t,(m)} \nabla \times (\boldsymbol{\tau}_q c_{m\phi}) - \frac{1}{j\omega\mu_0} \boldsymbol{\mu}_r^{-1} \sum_m \sum_q v_q^{\phi,(m)} \nabla \times \left(\mathbf{i}_\phi \frac{N_q}{\rho} s_{m\phi} \right). \tag{66}$$

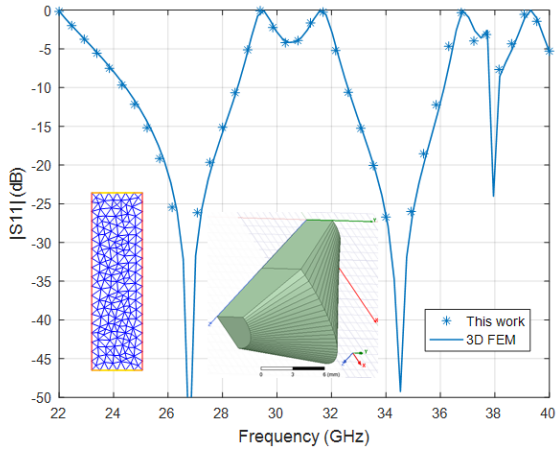

Fig. 1. Reflection coefficient of gradually varying section resonator. Input circular waveguide of radius 4 mm, resonator center semi-axes $a = 12$ mm, $b = 6$ mm, total length 14 mm.

IV. Results

In this section some results are shown for validation purposes and to quantify the efficiency of the new method discussed in this paper. All CPU times refer to a PC with Intel i7 processor with 4 GHz clock rate and 64 Gb RAM. The computer code for the analysis and design has been implemented in Matlab^{TM}. Further significant improvements are expected with a more efficiency-oriented scientific language. In the BoR-FEM implementation we used polynomial basis functions up to degree 3, with a well defined relationship between edge element order and nodal element order [17]. Accuracy is mainly related to three factors: element order (1st, 2nd or 3rd), mesh size and maximum index of circular harmonics M (it is recalled that only odd harmonics are used). Mesh size is represented by mesh density $F = \lambda_0/h_{\max}$, where $h_{\max}$ is the maximum edge length in the 2D mesh.

The first example we show is a resonator with gradually elliptical cross-section. The structure is shown in the inset of Fig. 1 (only 1/4 of the structure is shown). The total length of the resonator is 14 mm, it is fed by a circular waveguide of radius 4 mm and the resonator cross-section varies gradually from circular to elliptical. At the center ($z = 7$ mm), the semi-axes are $a = 12$ mm and $b = 6$ mm. The resonator is fed by the x-polarized TE_{11} mode in the circular waveguide. In Fig. 1 we show a comparison with 3D FEM over a wide band. The curve in Fig. 1 has been obtained with 2nd order elements, $F = 10$, $M = 5$ and the agreement is excellent. The analysis with our method took 0.16 sec/freq. In the figure, the mesh used for the analysis is also shown.

In order to demonstrate the good convergence and accuracy of the method, we show a reference table. The same structure in Fig. 1 has been analyzed at 28 GHz by varying the element order, the mesh density F and the maximum harmonic index M. The convergence for parameter $|S_{11}|$ (in dB) in the various cases is shown in Tab. I.

As a general observation, we found that, as expected, 1st order elements provide very slow convergence, whereas 3rd order elements perform best in terms of accuracy and efficiency [23]. As a quick comparison between the performance of 2nd order elements and 3rd order elements, the CPU time for 2nd order elements and $F = 10$ is roughly the same as that of 3rd order elements and $F = 6$, but accuracy is better for the latter.

TABLE I
Convergence of $|S_{11}|$ for the structure in Fig. 1 at 28 GHz. $F = \lambda_0/h_{\max}$, M maximum harmonic index.

1st order	$F = 5$	10	15	20
$M = 1$	-9.87	-19.28	-21.44	-23.16
3	-11.94	-35.57	-29.32	-24.12
5	-12.13	-35.33	-22.03	-18.78
7	-12.14	-34.37	-21.63	-18.45
9	-12.14	-34.34	-21.62	-18.44
11	-12.14	-34.34	-21.61	-18.44
2nd order	$F = 5$	10	15	20
$M = 1$	-23.58	-25.33	-25.84	-26.07
3	-25.90	-20.38	-19.62	-19.30
5	-20.42	-15.89	-15.26	-15.01
7	-20.14	-15.58	-14.96	-14.71
9	-20.13	-15.57	-14.95	-14.70
11	-20.13	-15.57	-14.95	-14.70
3rd order	$F = 5$	10	15	20
$M = 1$	-26.69	-26.41	-26.48	-26.50
3	-19.73	-19.25	-18.98	-18.88
5	-15.63	-14.93	-14.72	-14.66
7	-15.33	-14.63	-14.42	-14.36
9	-15.33	-14.63	-14.42	-14.36
11	-15.33	-14.63	-14.42	-14.36

A second example for validation refers to an elliptical horn fed by a circular waveguide. The horn cross-section varies gradually from circular to elliptical. The input radius is 4 mm, the output semi-axes are $a = 20$ mm and $b = 10$ mm and the horn length is 40 mm, corresponding to about 4λ at 26 GHz. The results for the scattering parameters of the two TE_{11} modes are shown in Fig. 2. The insets in the figure show the physical structure and the 2D mesh used for the analysis. We analyzed both polarizations, pol. 1 indicating x-directed electric field at the input and pol. 2, indicating y directed electric field at the input. The 3D FEM analysis was carried out with no symmetries and radiation boundaries have been placed around the horn. Owing to the rather large size of the model, the analysis took several hours, whereas with the method discussed in this paper the complete frequency response (20 points) was obtained in about eight minutes with $F = 8$, $M = 9$ and 3rd order elements. The same results in terms of scattering parameters could be obtained in 1 minute setting $M = 3$, with no appreciable difference in the curve, but an accurate computation of the radiation pattern requires more circular harmonics. The comparison of the radiation patterns is shown in Fig. 3 and 4. In spite of the imperfect behavior of radiation boundary that causes some oscillations in the curves obtained by 3D FEM, the agreement is good. For completeness we also show in Fig. 5 a curve representing the most sensitive radiation pattern as a function of M ($\phi = 0$ plane, Pol. 2). We note that a good convergence is obtained, a larger value of M is required.

A. PML performance

The performance of the newly developed PML are summarized in Fig. 6–7. An important parameter to be tested is the distance d of PML from the structure (see the inset in Fig. 6).

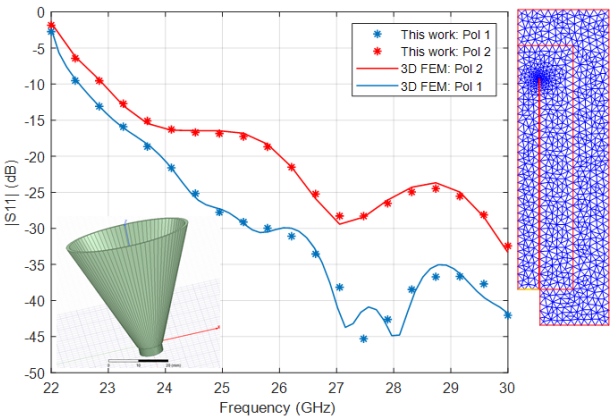

Fig. 2. Elliptical horn with axial ratio 2:1. Reflection coefficient for TE_{11}^{x} (Pol. 1) and TE_{11}^{y} (Pol. 2).

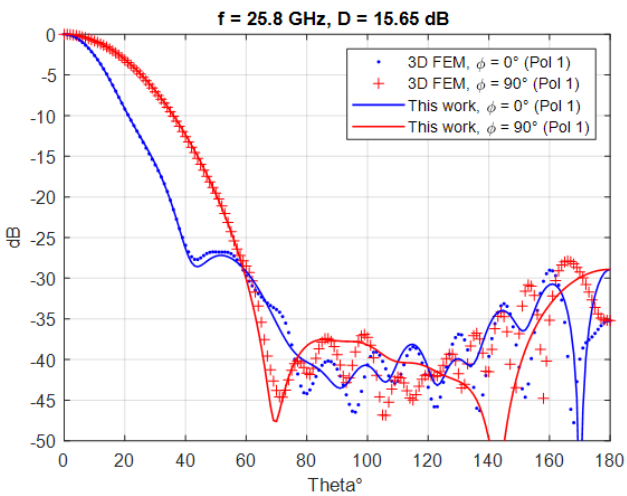

Fig. 3. Elliptical horn with axial ratio 2:1. Radiation pattern for TE_{11}^{x} (Pol. 1) at input.

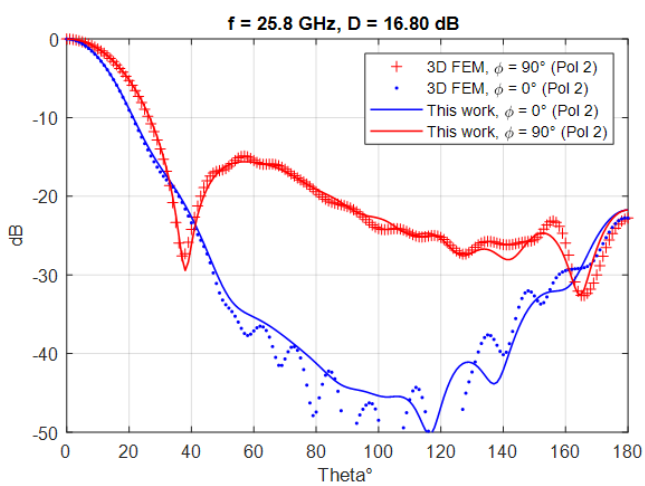

Fig. 4. Elliptical horn with axial ratio 2:1. Radiation pattern for TE_{11}^{y} (Pol. 2) at input.

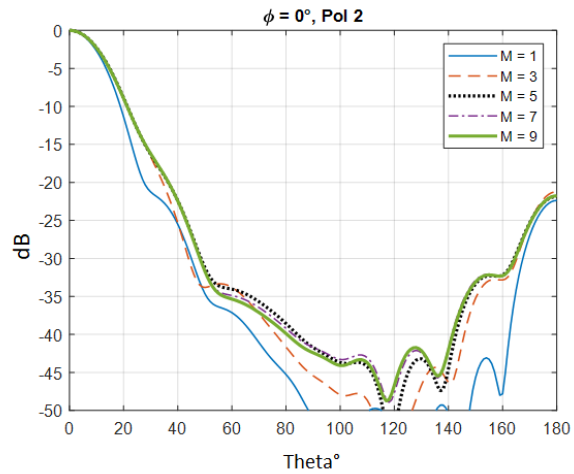

Fig. 5. Convergence of the most sensitive radiation pattern as a function of the maximum index of circular harmonics.

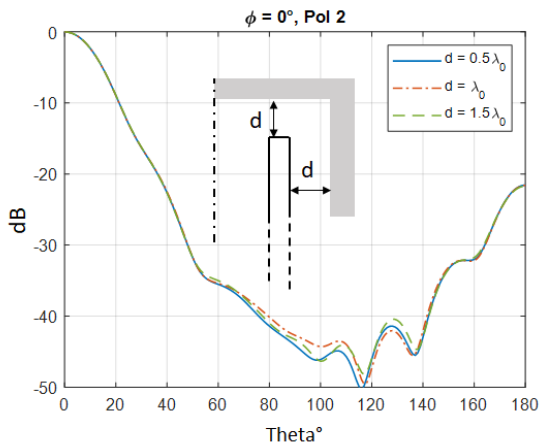

Fig. 6. Convergence of the most sensitive radiation pattern as a function of PML distance.

We show both horn pattern at 25.8 GHz, Pol. 2 (Fig. 6) and the reflection coefficient (Fig. 7), all other radiation patterns being less sensitive with respect to parameter d. One notes that in spite of the visible differences in Fig. 6, the performance of PML is very good. Reflection coefficient is also very stable even for values of d as small as 0.2λ (Fig. 7). The final value selected for computation is $d = \lambda/2$ as a good compromise between efficiency and accuracy.

B. Design curves

For design purposes, we carried out a parametric analysis on the relationship between gain and aperture size for different horn lengths and for the cases $a = 2b$ and $a = 3b$. The horn is excited by a circular waveguide and its cross section aspect ratio varies linearly from 1 to the final output aspect ratio. Both polarizations are considered. The results are shown in Fig. 8 for the case $a = 2b$ and in Fig. 10 for the case $a = 3b$. One notices the typical behavior of gain saturation because of phase error, but also a rather different behavior of the two polarizations. Similar curves have been derived for the maximum cross-polar level, computed according to Ludwig 3rd definition on plane $\phi = 45°$ and they are show in Figs. 9–

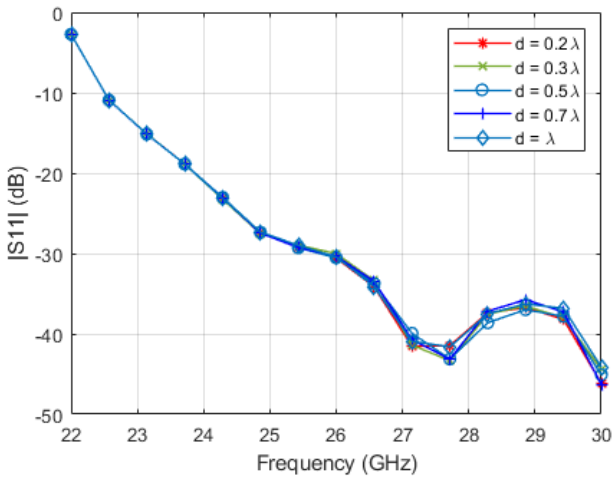

Fig. 7. Convergence of parameter S_{11} as a function of PML distance.

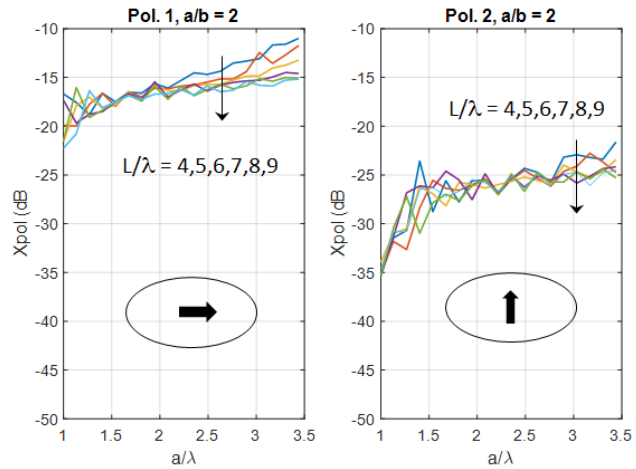

Fig. 9. Maximum cross-polar level as a function of aperture size with horn length L as a parameter, $a = 2b$.

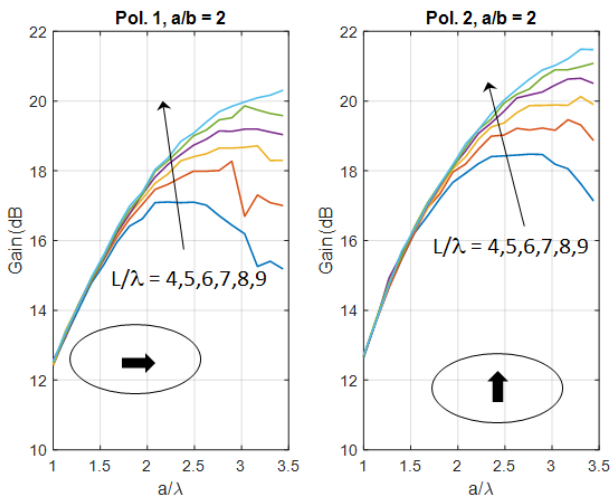

Fig. 8. Gain as a function of aperture size with horn length L as a parameter, $a = 2b$.

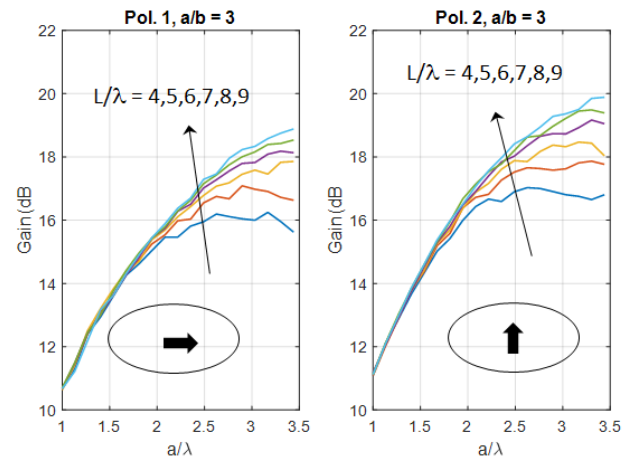

Fig. 10. Gain as a function of aperture size with horn length L as a parameter, $a = 3b$.

11. In this case the difference between the two polarizations is even more significant. Polarization 1 shows a much higher level of cross-polar component and this is slowly increasing with an increase in the normalized aperture size of the horn, with a moderate effect of horn length.

V. Conclusions

A new method based on Transformation Optics and 2D-FEM has been presented for the analysis of elliptical geometry structures. Application of the method to an elliptical resonator with variable ellipticity and to elliptical horns has demonstrated the accuracy and efficiency in the analysis. Newly developed PML conditions contributed to the excellent performance of the technique, with time reductions of 1 to 2 order of magnitudes with respect to full 3D techniques. Some design curves have been presented for the case $a = 2b$, showing both gain and cross-polar component.

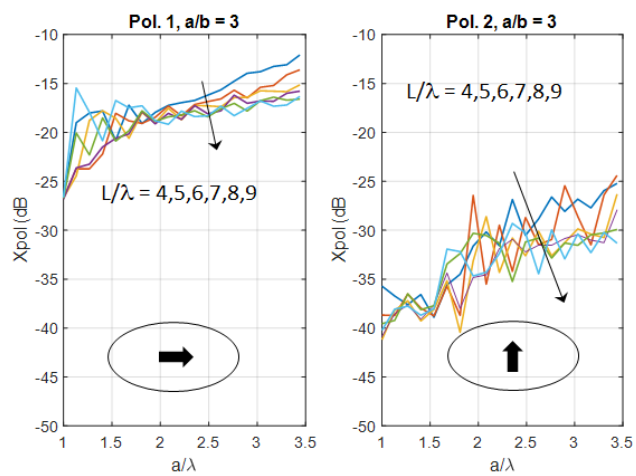

Fig. 11. Maximum cross-polar level as a function of aperture size with horn length L as a parameter, $a = 3b$.

APPENDIX

A. Matrix computation and storage

As shown in section III, FEM matrices are obtained as a product of integrals in (ρ, z) plane, times integrals in ϕ. The complete expression of the various terms is the following:

$$\mathbf{A}_{tt}^{(m,n)}(p,q) = \sum_i \sum_j \sum_k \int_S D_{\xi_i,p}^{t,(m)} V'_{(k)\xi_i\xi_j} D_{\xi_j,q}^{t,(n)} \rho d\rho dz \cdot \int_0^{2\pi} g_{i,m}^t V''_{(k)\xi_i\xi_j} g_{j,n}^t d\phi \tag{67}$$

$$\mathbf{A}_{t\phi}^{(m,n)}(p,q) = \sum_i \sum_j \sum_k \int_S D_{\xi_i,p}^{t,(m)} V'_{(k)\xi_i\xi_j} D_{\xi_j,q}^{\phi} \rho d\rho dz \cdot \int_0^{2\pi} g_{i,m}^t V''_{(k)\xi_i\xi_j} g_{j,n}^{\phi} d\phi \tag{68}$$

$$\mathbf{A}_{\phi t}^{(m,n)}(p,q) = \sum_i \sum_j \sum_k \int_S D_{\xi_i,p}^{\phi} V'_{(k)\xi_i\xi_j} D_{\xi_j,q}^{t,(n)} \rho d\rho dz \cdot \int_0^{2\pi} g_{i,m}^{\phi} V''_{(k)\xi_i\xi_j} g_{j,n}^t d\phi \tag{69}$$

$$\mathbf{A}_{\phi\phi}^{(m,n)}(p,q) = \sum_i \sum_j \sum_k \int_S D_{\xi_i,p}^{\phi} V'_{(k)\xi_i\xi_j} D_{\xi_j,q}^{\phi} \rho d\rho dz \cdot \int_0^{2\pi} g_{i,m}^{\phi} V''_{(k)\xi_i\xi_j} g_{j,n}^{\phi} d\phi. \tag{70}$$

Similarly, letting $\tau_{\xi_i,q}$ be the ξ_i component of vector basis τ_q

$$\mathbf{B}_{tt}^{(m,n)}(p,q) = \sum_i \sum_j \sum_k \int_S \tau_{\xi_i,p} \Lambda'_{(k)\xi_i\xi_j} \tau_{\xi_j,q} \rho d\rho dz \cdot \int_0^{2\pi} c_{m\phi} \Lambda''_{(k)\xi_i\xi_j} c_{n\phi} d\phi \tag{71}$$

$$\mathbf{B}_{t\phi}^{(m,n)}(p,q) = \sum_i \sum_k \int_S \tau_{\xi_i,p} \Lambda'_{(k)\xi_i\phi} N_q d\rho dz \cdot \int_0^{2\pi} c_{m\phi} \Lambda''_{(k)\xi_i\phi} s_{n\phi} d\phi \tag{72}$$

$$\mathbf{B}_{\phi t}^{(m,n)}(p,q) = \sum_j \sum_k \int_S N_q \Lambda'_{(k)\phi\xi_j} \tau_{\xi_j,p} d\rho dz \cdot \int_0^{2\pi} s_{m\phi} \Lambda''_{(k)\phi\xi_j} c_{n\phi} d\phi \tag{73}$$

$$\mathbf{B}_{\phi\phi}^{(m,n)}(p,q) = \sum_k \int_S N_q \Lambda'_{(k)\phi\phi} N_q \frac{1}{\rho} d\rho dz \cdot \int_0^{2\pi} s_{m\phi} \Lambda''_{(k)\phi\phi} s_{n\phi} d\phi. \tag{74}$$

B. Known term for circular waveguide excitation

The input magnetic field is expanded in circular waveguide modes. The know term matrix is therefore, for TE_{mn} modes

$$\mathbf{C}_t^{(m)}(q) = -\pi A_{mn} m \int_P \tau_{\rho,q} J_m(\chi'_{mn}\rho/b_1) d\rho \tag{75}$$

$$\mathbf{C}_\phi^{(m)}(q) = \pi A_{mn} \frac{\chi'_{mn}}{b_1} \int_P N_q J'_m(\chi'_{mn}\rho/b_1) d\rho \tag{76}$$

where J_m is the 1st kind Bessel function of order m, χ'_{mn} is the n-th zero of its derivative and $A_{mn} = |\frac{\pi}{2}(\chi_{mn}^2 - m^2) J_m(\chi'_{mn})^2|^{-1/2}$,. For TM_{mn} modes, we have

$$\mathbf{C}_t^{(m)}(q) = -\pi B_{mn} \frac{\chi_{mn}}{b_1} \int_P \tau_{\rho,q} J'_m(\chi_{mn}\rho/b_1) \rho d\rho \tag{77}$$

$$\mathbf{C}_\phi^{(m)}(q) = \pi B_{mn} m \int_P \frac{N_q}{\rho} J_m(\chi_{mn}\rho/b_1) d\rho \tag{78}$$

where χ_{mn} is the n-th zero of J_m and $B_{mn} = |\sqrt{\frac{\pi}{2}} \chi_{mn} J_{m+1}(\chi_{mn})|^{-1}$. Finally, P indicates integral over the port extension on the boundary. For an input elliptical waveguide, the fields are expanded in circular harmonics, see e.g. [24], [25].

REFERENCES

[1] P.J.B. Clarricoats and A.D. Olver, *Corrugated Horns for Microwave Antennas*, Peter Peregrinus Ltd, IEE Electromagnetic waves series 18, 1984.

[2] E. Lier, "Broad-band elliptical beamshape horns with low cross polarization," in IEEE Transactions on Antennas and Propagation, vol. 38, no. 6, pp. 800-805, Jun 1990.

[3] V.J. Vokurka, "Elliptical corrugated horn for broadcasting-satellite antennas," in Electronics Letters, vol. 15, no. 20, pp. 652-654, September 27 1979.

[4] D. Pujara, S.B. Sharma and S.B. Chakrabarty, "Computation of cross-polarization radiated by an elliptical feed horn," 2010 IEEE Antennas and Propagation Society International Symposium, Toronto, ON, 2010, pp. 1-4.

[5] A. Barka, O. Sguin and C. Breuil, "Design, fabrication and performance tests of elliptical antennas with low side lobe and coupling levels," Proceedings of the 2012 IEEE International Symposium on Antennas and Propagation, Chicago, IL, 2012, pp. 1-2.

[6] S. Amari and J. Bornemann, "A study of the symmetry of field patterns of elliptic horns fed by elliptic waveguides," IEEE Antennas and Propagation Society International Symposium. 1996 Digest, Baltimore, MD, USA, 1996, pp. 1992-1995 vol.3.

[7] E. Kuhn and A.S. Omar, "Complete characterization of corrugated elliptical horns for millimeter wave antennas," Radio Science Conference, 1998. NRSC '98. Proceedings of the Fifteenth National, Cairo, 1998, pp. INV1/1-INV1/9.

[8] C. Tomassoni, M. Mongiardo, E. Kuhn and A.S. Omar, "Generalized-Multipole-Technique - Mode-Matching-Technique Hybrid Method for Elliptical Stepped Horn Antennas Analysis," 2001 31st European Microwave Conference, London, England, 2001, pp. 1-4.

[9] C. Tomassoni, A.S. Omar and M. Mongiardo, "A novel closed-form formula for radiation pattern evaluation of elliptical horn antennas," 2002 32nd European Microwave Conference, Milan, Italy, 2002, pp. 1-4.

[10] G. Pelosi, R. Coccioli, S. Selleri, *Quick Finite Elements for Electromagnetic Waves*, 2nd edition, 2009, Artech House.

[11] M. Mongiardo and C. Tomassoni, "Modal analysis of discontinuities between elliptical waveguides," in IEEE Transactions on Microwave Theory and Techniques, vol. 48, no. 4, pp. 597-605, Apr 2000.

[12] P. Matras, R. Bunger and F. Arndt, "Mode-matching analysis of the step discontinuity in elliptical waveguides," in IEEE Microwave and Guided Wave Letters, vol. 6, no. 3, pp. 143-145, Mar 1996.

[13] A.I. Dimitriadis, M. Favre, M. Billod, J.P. Ansermet and E. de Rijk, "Design and fabrication of a lightweight additive-manufactured Ka-band horn antenna array," 2016 10th European Conference on Antennas and Propagation (EuCAP), Davos, 2016, pp. 1-4.

[14] O.A. Peverini et al., "Selective Laser Melting Manufacturing of Microwave Waveguide Devices," in Proceedings of the IEEE, vol. 105, no. 4, pp. 620-631, April 2017.

[15] N.B. Kundtz, D.R. Smith and J.B. Pendry, "Electromagnetic Design With Transformation Optics," in Proceedings of the IEEE, vol. 99, no. 10, pp. 1622-1633, Oct. 2011.

[16] A. D. Greenwood and Jian-Ming Jin, "A novel efficient algorithm for scattering from a complex BOR using mixed finite elements and cylindrical PML," in IEEE Transactions on Antennas and Propagation, vol. 47, no. 4, pp. 620-629, Apr 1999.

[17] G.G. Gentili, P. Bolli, R. Nesti, G. Pelosi and L. Toso, "High-Order FEM Mode Matching Analysis of Circular Horns With Rotationally Symmetric Dielectrics," in IEEE Transactions on Antennas and Propagation, vol. 55, no. 10, pp. 2915-2918, Oct. 2007.

[18] A. Keivaan, M.H. Fakheri, A. Abdolali and H. Oraizi, "Design of Coating Materials for Cloaking and Directivity Enhancement of Cylindrical Antennas Using Transformation Optics," in IEEE Antennas and Wireless Propagation Letters, vol. 16, pp. 3122-3125, 2017.

[19] R.C. Mitchell-Thomas, M. Ebrahimpouri and O. Quevedo-Teruel, "Altering antenna radiation properties with transformation optics," 2015 9th European Conference on Antennas and Propagation (EuCAP), Lisbon, 2015, pp. 1-2.

[20] A.P. Smull, A.B. Mani, S.B. Mani and B.M. Notaro, "Anisotropic Locally Conformal Perfectly Matched Layer for Higher Order Curvilinear Finite-Element Modeling," in IEEE Transactions on Antennas and Propagation, vol. 65, no. 12, pp. 7157-7165, Dec. 2017.

[21] F. L. Teixeira and W.C. Chew, "Systematic derivation of anisotropic PML absorbing media in cylindrical and spherical coordinates," in IEEE Microwave and Guided Wave Letters, vol. 7, no. 11, pp. 371-373, Nov 1997.

[22] A.E.H. Love, "The Integration of Equations of Propagation of Electric Waves", Phil Trans. Roy. Soc. London, Ser. A, 197, 1901, pp. 1–45.

[23] R.D. Graglia, D. R. Wilton and A.F. Peterson, "Higher order interpolatory vector bases for computational electromagnetics," in IEEE Transactions on Antennas and Propagation, vol. 45, no. 3, pp. 329-342, Mar 1997.

[24] G.G. Gentili, R. Nesti, G. Pelosi and S. Selleri, "A perturbative approach for the determination of modes in slightly elliptical waveguides", 2017 International Conference on Electromagnetics in Advanced Applications (ICEAA), Verona, 2017, pp. 653-656.

[25] G. G. Gentili, G. Pelosi, S. Selleri, "A line integral perturbative approach to the computation of cutoff frequencies in deformed waveguides," IEEE Microwave Wireless Components Letters, Vol. 25, No. 7, June 2015, pp. 421-423.